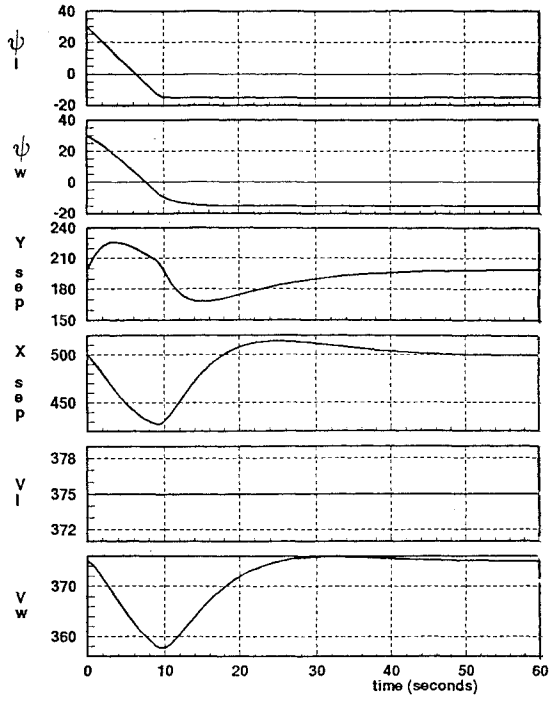

Fig. 3 Time response plots for diamond leader-wingman formation.

out, the initial formation velocity and the initial formation spacing are maintained in steady state. Therefore, the formation geometry is maintained after the heading change maneuver is completed and there is no danger of an L/W collision during the transition process.

VII. Conclusions

The control design problem of an automatic pilot for formation flight control has been analyzed and decomposed into two uncoupled linear single-input, two-output dynamic tracking control system design problems, which correspond to the y and x channels, respectively. This, in turn, results in the efficient design of a PI formation-hold autopilot that uses a mix of separation errors and maneuver errors. The formation-hold autopilot is an extension of the conventional heading-hold and Mach-hold autopilots. However, the formation control problem involves two flight vehicles and their accurate relative positions.

The formation flight control problem considered here is significant in view of its direct operational importance: It affords the automation of the coordination of a leader/wingman flight, the design of a robotic wingman, and the automatic control of aircraft during maneuvers such as aerial refueling. It is also interesting in view of the novel and nontrivial control theoretic problems that it poses.

References

[1]Wellinger, D., "Army Formation Flight Study: Final Report," Contract No. DA-36-039-ACM-03367(E), Radio Corporation of America, Burlington, MA, Feb. 1965.

[2]Rohs, P. R., "A Fully Coupled, Automated Formation Control System for Dissimilar Aircraft in Maneuvering, Formation Flight," M.S. Thesis, AFIT/GE/ENG/91M-03, Air Force Inst. of Technology, Wright-Patterson AFB, OH, March 1991.

[3]Dargan, J. L., "Proportional Plus Integral Control of Aircraft for Automated Maneuvering Formation Flight," M.S. Thesis, AFIT/GE/ENG/ 91D-14, Air Force Inst. of Technology, Wright-Patterson AFB, OH, Dec. 1991.

[4]Dargan, J. J., Pachter, M., and D'Azzo, J. J., "Automatic Formation Flight Control," *Proceedings of the AIAA Guidance, Navigation and Control Conference* (Hilton Head, SC), AIAA, Washington, DC, 1992, pp. 836–857 (AIAA Paper No. 92-4473).

[5]Porter, B., and Bradshaw, A., "Design of Linear Multivariable Continuous-Time Tracking Systems," *International Journal of System Science*, Vol. 5, 1974, pp. 1155–1164.

[6]Porter, B., and Bradshaw, A., "Singular Pertubation Methods in the Design of Tracking Systems Incorporating Inner-Loop Compensators and High-Gain Error-Actuated Controllers," *International Journal of System Science*, Vol. 12, 1981, pp. 1193–1205.

[7]Buzogany, L. E., Pachter, M., and D'Azzo, J. J., "Automated Control of Aircraft in Formation Flight," *Proceedings of the AIAA Guidance, Navigation and Control Conference* (Monterey, CA), AIAA, Washington, DC, 1993, pp. 1349–1370 (AIAA Paper No. 93-3852).

Drag Function Modeling for Air Traffic Simulation

Mark R. Anderson*
Virginia Polytechnic Institute and State University, Blacksburg, Virginia 24061
and
Daniel E. Schab†
Naval Air Warfare Center, Orlando, Florida 32826

Introduction

In most modern aircraft training simulators, many aircraft are being flown simultaneously to mimic surrounding air traffic. For combat simulators, the flight performance fidelity of the aircraft traffic or threat environment is particularly important for effective combat tactics training. The air traffic models must also be very simple so that a minimum amount of computational power is used during these real-time simulations.

Most air traffic models in use today have been developed by piecing together manufacturer's data into a simplified model of the aircraft. However, for many aircraft, data may be available in the form of performance charts. Excess power contours and energy maneuverability charts are estimated for many aircraft to make comparisons between different aircraft types. These performance predictions are a valuable source of information that can be used for air traffic simulation modeling.

This note offers a new approach to developing a drag function expression for commercial air traffic or combat aircraft threat models. The idea is to determine parameters of a simplified drag coefficient function so that the performance of the modeled aircraft closely matches that of the actual aircraft. The drag function parameters are varied using a form of parameter identification or multidimensional curve fitting. In other words, the parameters of the air traffic model drag function are actually extracted from performance data rather than estimated from wind tunnel data. Thus, the performance of the air traffic model will match the actual aircraft.

Drag Error Function Structure

Most air traffic models are based upon energy state equations of motion.[1–5] The excess power or rate of change of energy is given by

$$P_s = \frac{\mathrm{d}E}{\mathrm{d}t} = \frac{V(T-D)}{W} \tag{1}$$

where $E = h + V^2/2g$ is specific energy, h is altitude, V is velocity, W is weight, and P_s is excess power. The axial forces acting on the

Received Nov. 6, 1993; revision received April 8, 1994; accepted for publication April 14, 1994.

*Assistant Professor, Department of Aerospace and Ocean Engineering. Senior Member AIAA.

†Aerospace Engineer, Training Systems Division, Fighter Attack Branch. Member AIAA.

vehicle are the maximum available engine thrust T and drag D. The primary modeling emphasis is the drag force D. It is easiest to model this function using a simple drag polar, given by

$$D = qSC_D = qS\left(C_{D_0} + KC_L^2\right) \tag{2}$$

where q is dynamic pressure, S is a reference area, and C_L is lift coefficient.

For high speed combat aircraft, the drag polar is not sufficient to accurately model the drag characteristics of the aircraft. As a result, the performance of the combat models usually will not match the performance of the actual aircraft at high subsonic or supersonic speeds. To include the effect of Mach number, a drag coefficient represented by the following function is considered:

$$C_D = C_{D_0} + KC_L^2 + f(C_L, M) \tag{3}$$

The error function $f(C_L, M)$ is intended to take on many forms. Its primary purpose is to model any differences between a simple drag polar and the drag coefficient function needed to match the performance of the actual aircraft. However, since a very simple thrust model is assumed, the drag error function also accounts for differences between the thrust model and the actual aircraft propulsion system.

Although many other forms are possible, the error function $f(C_L, M)$ is represented herein in terms of a weighted sum of cubic spline basis functions

$$f(C_L, M) = \sum_{i=1}^{n_c+2} \sum_{j=1}^{n_m+2} b_{ij}\xi_i(C_L)\xi_j(M) \tag{4}$$

with $\xi(\cdot)$ representing a single spline basis function and n_c and n_m are the number of spline nodes or "knots" in C_L and Mach number, respectively. The individual spline functions are defined as in Ref. 6. The parameters that are fitted to performance data are the spline coefficients b_{ij} in Eq. (4). The number of spline function coefficients depends upon the number of spline knots used. From Eq. (4), one can see that there will be $(n_c + 2) \times (n_m + 2)$ spline function coefficients. The principal advantage of the spline function representation is that greater or less fidelity can be obtained by changing the number of spline knots used in the procedure (with a corresponding increase or decrease in computational requirements).

Drag Error Coefficient Parameter Identification

Level, straight, and turning flight excess power contour plots can be digitized to yield data points of Mach number M, altitude, and excess power. The excess power data are then converted to equivalent lift and drag coefficients using the following expressions:

$$C_D = \frac{2(W/S)}{\rho(Ma)^2}\left(\frac{\delta T_0}{W} - \frac{P_s}{Ma}\right) \tag{5}$$

$$C_L = \frac{2n(W/S)}{\rho(Ma)^2} \tag{6}$$

where a is the speed of sound, n is the load factor, ρ is the atmospheric density, δ is the density ratio ($\delta = \rho/\rho_{SL}$), W/S is the aircraft's wing loading, and T_0 is the maximum sea level static engine thrust. The propulsion system thrust usually depends upon altitude and Mach number. To approximate the effect of altitude, the engine thrust in Eq. (5) is assumed to vary with density ratio such that $T = \delta T_0$.

The drag function modeling is completed in two steps. In the first step, only the drag polar parameters C_{D_0} and K are determined by assuming $f(C_L, M) = 0$. The resulting drag polar model usually results in a fairly good subsonic model. For improved fidelity, a second identification is then carried out to determine the drag coefficient error function parameters. The second step is to fit the spline coefficients that make up the error function $f(C_L, M)$. To determine the spline coefficients, the data fitting scheme proposed in Ref. 6 is recommended.

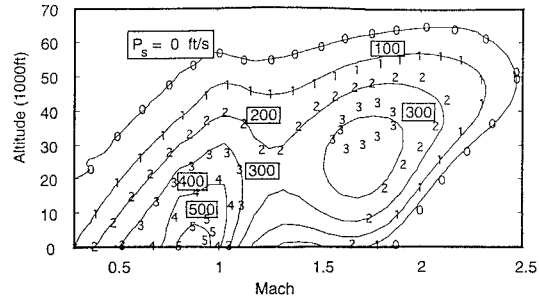

Fig. 1 F-104G drag function model contours of constant excess power.

There are two design choices that must be made prior to computing the spline function coefficients. First, the spline knot locations for C_L and Mach number must be selected. The spline knots generally should be chosen wherever the drag function undergoes significant variations. For example, it is often helpful to specify several tightly spaced knots near Mach 1 in order to correctly model drag rise. The singular-value threshold (see Ref. 6) should be chosen as small as possible to yield good model fidelity. However, a threshold set too small will result in a drag coefficient function that is unrealistically complex due to ill-conditioning.

Finally, one should note that the drag function that is extracted from the aircraft performance data does not necessarily represent the actual drag acting on the aircraft. The fitted drag function not only includes errors due to the fitting procedure, but it also includes the errors inherent in the simplified engine thrust model. In particular, the drag error function will contain thrust variations in Mach number that are not at all represented in the simplified expression for thrust. However, separating thrust effects from the performance data allows the simulation engineer to add other propulsion system characteristics such as a throttle, rate limits, and simplified dynamics.

Example

Figure 1 shows contours of excess power for the Lockheed F-104G supersonic jet in level flight. The numbered symbols in the figure represent the actual performance data for the aircraft. A 0 represents $P_s = 0$ ft/s, 1 represents $P_s = 100$ ft/s, etc. These 106 data points were electronically digitized from the contour plot presented in Ref. 7. A weight $W = 18,000$ lb, reference area $S = 195$ ft^2, and maximum static sea level thrust $T_0 = 15,800$ lb were assumed.

The solid lines in Fig. 1 show the excess power performance fidelity that is obtained after drag model fitting. These curves are created by computing the excess power from Eq. (1) using the drag function model from Eq. (3) and a grid of altitude and Mach number pairs. Comparing the solid lines to the numbered symbols indicates that the performance of the model is quite good, even at high speed. The spline knots were chosen for C_L at [0.0 0.2 0.6 1.1] and Mach number at [0.3 0.8 0.9 1.1 1.2 1.6 2.0 2.5]. Better matching fidelity can be obtained using more spline knots; however, more spline knots will also result in a greater number of function parameters and reduced computational efficiency. A total of 62 parameters are needed to model this drag function. A singular-value threshold of 0.01 was chosen for this example.

Conclusions

The example results shown in this note reveal that surprisingly detailed drag coefficient functions can be extracted directly from typical aircraft performance charts. The performance of the resulting model closely matches that of the actual aircraft. The parameter-fitting method used in the modeling procedure has only a limited number of design choices; therefore, the level of engineering expertise required and the time needed to develop new aircraft models should be significantly reduced. Finally, by simply changing the drag error function, air traffic models can be easily modified or upgraded whenever new performance estimates are obtained.

Acknowledgments

The research reported in this note was sponsored by the Naval Air Warfare Center, Training Systems Division, under Contract

N61339-92-C-0100, and the Naval Air Systems Command. The authors thank R. Thomas Galloway for helping to define the research objectives. The authors are also grateful to Brent York, Chris Weekley, and David Honaker for their help in developing the drag function modeling software.

References

[1]Kelley, H. J., "Reduced-Order Modeling in Aircraft Mission Analysis," *AIAA Journal*, Vol. 9, No. 2, 1971, pp. 349, 350.

[2]Burgin, G. H., et al., "An Adaptive Maneuvering Logic Computer Program for the Simulation of One-on-One Air-to-Air Combat, NASA CR-2582, Sept. 1975.

[3]Williams, D. H., and Wells, D. C., "Traffic Scenario Generation Technique for Piloted Simulation Studies," NASA TM-86397, April 1987.

[4]Miralles, C. T., Selmon, J., and Trujillo, S. M., "An Air Combat Simulation Model Suitable for the Evaluation of Agility and EFM," AIAA Paper 89-3311, Aug. 1989.

[5]Goodrich, K. H., and McManus, J. W., "Development of a Tactical Guidance Research and Evaluation System (TiGRES)," AIAA Paper 89-3312, Aug. 1989.

[6]Cloutier, J. R., "Multivariate, Minimum-Curvature Splines for Randomly-Space Data," AIAA Paper 91-2744, Aug. 1991.

[7]Anderson, J. D., *Introduction to Flight*, McGraw-Hill, New York, 1989.

Autonomous Spacecraft Gyro Failure Detection Based on Conservation of Angular Momentum

F. Landis Markley*
NASA Goddard Space Flight Center, Greenbelt, Maryland 20771
Kevin R. Kennedy† and John D. Nelson‡
Lockheed Missiles and Space Company, Inc., Sunnyvale, California, 94088
and
Edward W. Moy§
Lockheed Technical Operations Company, Greenbelt, Maryland, 20770

Introduction

THIS note describes a new gyro failure detection algorithm implemented onboard the Hubble Space Telescope (HST) to detect a class of potential gyro failures that would not have been recognized by pre-existing failure detection algorithms. This test is called the system momentum test, since it detects failures by monitoring the change in the system momentum calculated in the flight computer.

The HST was launched with six primary single-degree-of-freedom high-accuracy gyros for redundancy. The science pointing mode of the HST normally uses four gyros to provide gyro fault detection and improved smoothing of gyro noise, but good pointing performance (with reduced fault detection capability) is possible with three gyros.[1-3] The spacecraft is uncontrollable in this pointing mode with only two gyros, due to the unobservability of a body rate perpendicular to the input axes of both gyros, but vehicle health and safety can still be maintained with either the Zero Gyro Sunpoint safemode in the flight computer[4] or the hardware sunpoint capability using the Pointing and Safemode Electronics Assembly and the lower accuracy retrieval mode gyros.

The original fault detection logic in the HST flight computer monitored three types of gyro failures: a) disparity between measured and expected gyro counts, b) off-nominal values of hardware gyro error indicator bits, and c) measured gyro counts exceeding saturation limits. Unfortunately, these tests cannot detect a gyro failure that results in a near-zero gyro output independent of the actual spacecraft body rate when the commanded rate is also near zero. A gyro failure of this type, termed a "soft" gyro failure, could result from a failure of the rotor drive mechanism, for example. Any configuration of four gyros provides redundant information about individual vehicle axes, so a soft failure of one gyro would not have serious consequences; the three remaining gyros would allow computation of inaccurate but acceptable body rate information until one of the above tests caused the failed gyro to be autonomously removed from use. However, a soft gyro failure from a three-gyro configuration would cause an undetected increase in the vehicle angular velocity about an insensitive axis that the failed gyro would normally sense. In fact, the spacecraft attitude control system would attempt unsuccessfully to drive the output of the failed gyro to an exact zero rate, forcing the undetected rate to increase rapidly. A simulation of a soft gyro failure in the HST hardware/software interface facility verified that the existing safemode tests would not detect such a failure and that the spacecraft rate about the undetected axis would rapidly increase to a level high enough to endanger spacecraft health.

The inability of the existing gyro failure detection tests to detect a soft failure—and the threat of such a failure on the HST—led to the addition of the system momentum test. This test allows reliable and rapid detection of a soft gyro failure by checking the change in the system momentum calculated in the flight computer. In the event of such a failure, the control system response to incorrectly measured body rates causes a rapid change in computed system momentum. The system momentum test triggers a safemode entry upon detecting this change.

Simultaneous soft failures of two gyros from a four-gyro configuration is possible but improbable, since it requires a minimum of three hardware component failures in the shared clock controlling the two gyros. Although this failure mode has never occurred, simulations show that the result would be detected by the system momentum test.

System Momentum Test Algorithm

Changes in the total system momentum

$$\boldsymbol{H} = I\boldsymbol{w} + \boldsymbol{H}_{\mathrm{RW}} \tag{1}$$

are caused only by external disturbance torques such as aerodynamic drag and gravity gradient torques. In Eq. (1), I is the vehicle moment of inertia tensor, $\boldsymbol{w}$ is the vehicle angular velocity, and $\boldsymbol{H}_{\mathrm{RW}}$ is the reaction wheel angular momentum in the vehicle frame. Internal reaction wheel torques are balanced by Newton's third law so that any change in the spacecraft body angular momentum is balanced by an equal and opposite change in the momentum of the reaction wheels, resulting in zero net change in the system momentum. Since the external torques are small, the system momentum is slowly changing.

The system momentum is calculated in the flight computer for use in compensating gyroscopic torques and for momentum management. If any of the quantities entering into this computation is incorrect, the computed system momentum may change rapidly, with a rate of change much larger than the external disturbance torques. This is the basis of the system momentum test for soft gyro failures. This test estimates the net unmodeled environmental torque as

$$\boldsymbol{T}_{\mathrm{est}} = \frac{\mathrm{d}\boldsymbol{H}}{\mathrm{d}t} + \boldsymbol{w} \times \boldsymbol{H} - \boldsymbol{m} \times \boldsymbol{B} - \boldsymbol{T}_{\mathrm{gg}} \tag{2}$$

where $\boldsymbol{w} \times \boldsymbol{H}$ is the gyroscopic torque, $\boldsymbol{m} \times \boldsymbol{B}$ is the commanded magnetic torque, and $\boldsymbol{T}_{\mathrm{gg}}$ is an estimate of the gravity gradient torque. If all sensors are operating properly, the magnitude of $\boldsymbol{T}_{\mathrm{est}}$ will be on

Received Sept. 28, 1993; revision received Jan. 13, 1994; accepted for publication Feb. 5, 1994.

*Staff Engineer, Guidance and Control Branch, Code 712. Associate Fellow AIAA.

†Research Engineer Senior.

‡Group Engineer. Member AIAA.

§Staff Engineer.